"Structural and Optical Studies on Phosphorous doped TiO_2 nanoparticles"

Sandip B. Deshmukh[a*], Dhananjay V. Mane[b], Mangesh G. Bhosale[a], Maheshkumar L. Mane[c], Jalindar D. Ambekar[d]

a. *Department of Chemistry, Ramkrishna Paramhansa Mahavidyalaya, Osmanabad. 413 501, Maharashtra, India.*
b. *Department of Chemistry, Shri Chhatrapati Shivaji Mahavidyalaya, Omerga 413 606, Maharashtra, India.*
c. *Department of Physics, Shikshan Maharshi Guruvarya R. G. Shinde Mahavidyalaya, Paranda 413 502, Maharashtra, India.*
d. *Centre for Materials for Electronics Technology (C-MET), Pune 411 008, Maharashtra, India.*

**Corresponding author*

Abstract

The pure anatase phase tetragonal structured Phophorous doped TiO_2 nanoparticles were successfully synthesized at room temperature by using simple sol–gel method. The structural, optical properties of the materials are investigated thoroughly by various spectral techniques (XRD, EDAX, FT-IR, and UV-DRS) and electron microscopy (FESEM and HRTEM). The experimental results suggest that, the P doped TiO_2 influenced the structural, morphological, and optical properties significantly. UV-DRS studies investigate that the doping of P ion can directly shift band gap of semiconductors into the visible region. The energy band gap decreases from 3.2 to 2.0 eV as the doping of mole % of P increases as 1, 3 and 5 mole %. P doping can effectively decrease the recombination rate of photogenerated charges in TiO_2.

1. Introduction

Heterogeneous photocatalysis has shown distinctive advantages in degradation [1]. TiO_2 semiconductor is extensively used as raw materials of ointment, paint, sunscreen, and toothpaste [2- 4]. Semiconductor photocatalysis has attracted wide attention in the field of water splitting, CO_2 reduction and pollution degradation [5-12] after the Honda and Fujishima's discovery of water photolysis on TiO_2 [13]. Now days, TiO_2 is still regarded as one of the most significant photocatalysts due to its long-term stability, low cost and nontoxicity [14-15]. However, the exploitation of visible light is limited due to the large band gap. The band gap of anatase TiO_2 is 3.2 eV and it is in the UV region. Moreover, the high resistance and high carrier recombination rate are also the disadvantages of TiO_2 photocatalyst [15,16]. To enhance the lifetime of photogenerated electron–hole pairs and decrease the band gap, various methods and techniques have been developed such as metal ion and nonmetal ion doping[17,18], with several foreign ions[19, 20], hybridization with carbon materials[21,22], co-doping, and surface sensitization by noble metal [23]. Nonmetal ion doping has made great success in the field of modifying photocatalyst such as N [24 – 27] and S [28-30]. The doping of nonmetal ion can directly shift

band gap of semiconductors, resulting improved visible excited photocatalytic efficiency [31-33]. Comparing with other nonmetal elements, phosphorus has distinctive advantages on improving photocatalytic efficiency. P doping can effectively decrease the recombination rate of photogenerated charges in TiO_2 [34,35]. On the other hand, it has been reported by many researchers that moderate oxygen vacancies on photocatalyst can result in the formation of unpaired electrons and avoid the electron hole recombination [36, 37].

2 Materials and method

2.1 Materials

Nanocrystalline P doped TiO_2 was synthesized by using the sol-gel technique. In this work Analytical grade titanium(IV)tetraisopropoxide (TTIP) ($TiOCH(CH_3)_{24}$ 97% Sigma Aldrich), Orthophosphoric acid (H_3PO_4), Oleic acid ($C_{18}H_{34}O_2$), ammonia (NH_3) and absolute ethyl alcohol (C_2H_5OH) were used for the synthesis.

2.2 Synthesis of P doped TiO_2 nanoparticles

Optimum compositions (0.0 mole %, 1 mole %, 3 mole % and 5 mole %) of P doped TiO_2 nanoparticles were prepared by sol-gel method at room temperature.

5ml Oleic acid was taken in a 250 mL round-bottom flask. The content was stirred at 120^0C for 10 min. followed by the addition of 10 mL TTIP and 200 mL distilled water (DW); white precipitate of titanium hydroxide was formed. The content was stirred at room temperature for 1 h. Then, the content was filtered and re-slurred in 200 mL DW and the pH of the solution was adjusted to 10 by using an ammonia solution. After that, the content was stirred at 60^0C for 3 h. The stoichiometric quantity of orthophosphoric acid (H_3PO_4) was added into the above solution. The content was again stirred for 3 h at 60^0C. Then, the content was filtered and washed with 50 mL DW and 10 mL ethyl alcohol. After that, the residue was dried at 100^0C and annealed in air at 500^0C for 5 h. After annealing, the residue resulted in the off white colored P doped TiO_2 nanoparticles.

2.3 Characterization

The prepared powder samples were characterized by powder X-ray diffraction technique. XRD data of the samples were collected in the 2θ range of $10^0 – 90^0$ in step scan mode at a rate of 0.2^0/min using ULTIMA IV, Rigaku Corporation, Japan diffractometer with source Cu Kα (Kα1 = 1.5406 and Kα1 = 1.5444 Å) radiation. Nicolet iS10, Thermo Scientific, USA Fourier Transform Infrared spectrometer was used to record FTIR spectra of the nanoparticles in the range of 400 cm^{-1} to 4000 cm^{-1} with the transmission mode. The surface morphology of samples was investigated by using filed emission Scanning Electron Microscopy (FE-SEM) Hitachi S-4800 system with EDAX analysis was performed to determine the elemental composition of the samples. A JEOL JEM2100F field emission gun-transmission electron microscope (HR-TEM 200kV) operating at 200 kV with resolution (Point: 0.19 nm Line: 0.1 nm) and magnification (50X – 1.5 X) was employed for generating HR-TEM image of the nanoparticles. UV–Visible diffuse reflectance spectra of all the samples were recorded in the range of 200 nm – 800 nm, using an ELICO – SL159 UV–Visible spectrometer.

3 Results and discussion

3.1 X-ray diffraction analysis (XRD)

Figure 1 suggests the phase formation and crystalline structure of bare TiO_2 and various concentrations of P doped TiO_2 nanoparticles X-ray diffraction analysis was performed on the precursor material at room temperature using Cu-Kα radiations (λ=1.5406 Å). Fig. 4.11 shows XRD spectra of all the samples. The X-ray diffraction peaks (101), (004), (200), (105), (211),

(204), (116), (220), and (215) of bare TiO_2 corresponding to diffraction angles at 2θ = 25.4°, 38.02°, 48.14°, 54.12°, 55.18°, 62.81°, 68.71°, 70.28°, and 75.30° could be attributed to the anatase phase TiO_2, respectively (JCPDS 21-1272). No peak phase assigned to P was observed with doping concentration, the crystal structure of doped TiO_2 samples shows stability of anatase phase when compared with that of bare TiO_2 sample. The average crystallite size of all the samples was calculated from the Full Width at Half Maximum (FWHM) (β) of all major diffraction peaks of anatase, using the Debye-Scherer method [38]. The obtained results of the average crystallite size (D) changed after P doping was tabulated in **Table 1**. The variation of crystallite size with P mole% was shown in **Figure 2** and it is observed that due to P doping crystallite size decreases.

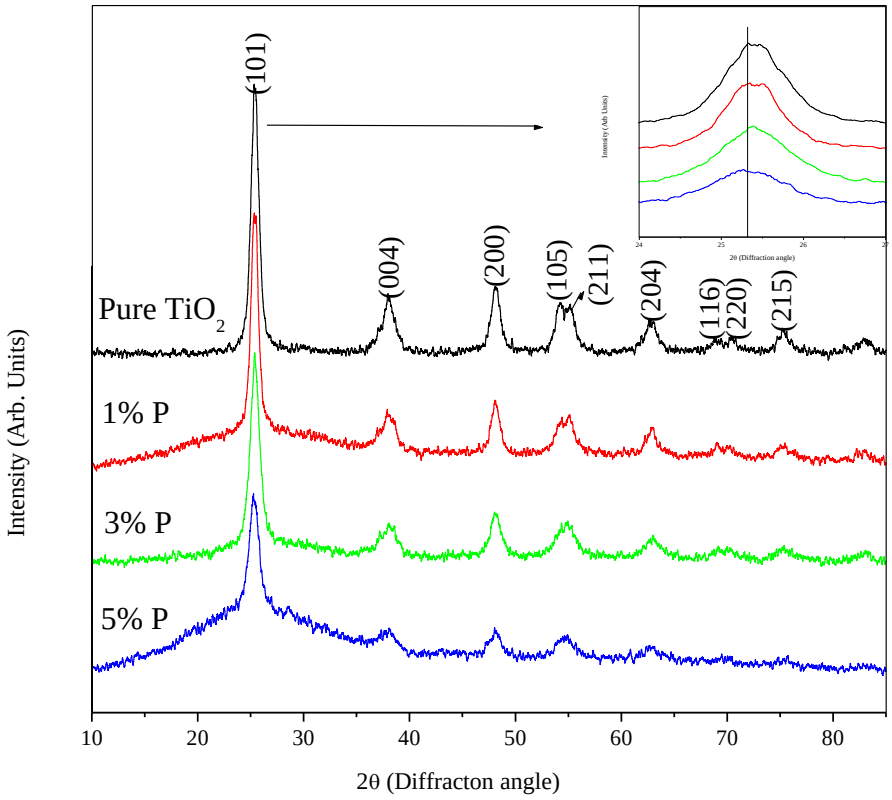

Figure 1: X-ray Diffraction Pattern for bare TiO_2 and P-doped TiO_2 nanoparticles

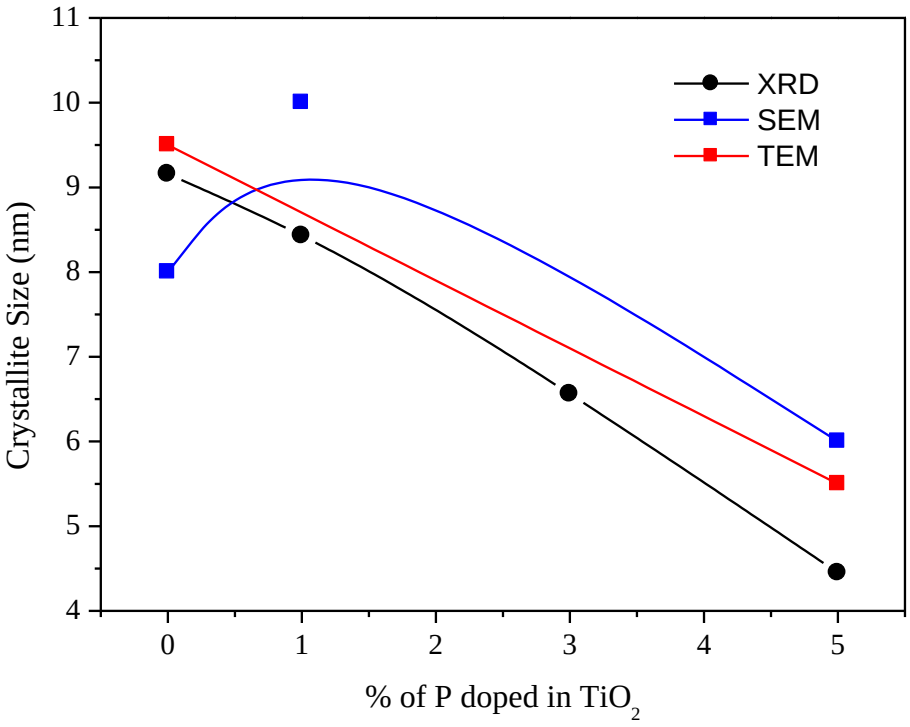

Figure 2: Variation of crystallite size with % of P doped in TiO_2 nanoparticles

Table 1: The average crystallite size

Bare TiO2			1 % P			3 % P			5 % P		
2θ	β	D (nm)	2θ	β	D (nm)	2θ	β	D (nm)	2θ	β	D (nm)
25.41	0.81	10.03	25.38	0.89	9.14	25.41	1.10	7.38	25.19	2.97	2.74
38.03	1.28	6.58	37.95	1.56	5.39	38.00	1.67	5.03	27.97	1.62	5.07
48.14	0.91	9.53	48.12	0.83	10.52	48.14	1.07	8.16	48.10	1.45	5.99
54.13	0.79	11.34	54.74	1.53	5.86	54.76	1.73	5.19	54.70	2.23	4.02
62.81	1.16	8.01	62.84	0.83	11.26	62.96	1.32	7.05			
Average D (nm)		9.10			8.43			6.56			4.45

3.2 Fourier transform infrared spectroscopy (FTIR)

The FTIR spectra of bare and 1, 3 and 5 mole% P are shown in **Figure 3**. The FTIR of bare and various mole% of TiO_2 shown broad bands at 3240 and 1640 cm^{-1} is corresponding to the -OH stretching and bending vibrations of chemical adsorbed water and hydroxyl groups [39]. As the mole% of P increases, these bands became broader and stronger than that for the bare TiO_2 [40]. The P doping is responsible for high adsorption capacity of the TiO_2 due to their large surface area. The absorption bands shown at 1040, 1095, and 1125 cm^{-1} is attributed to the doped materials, signifying the chemical environment of the P in the TiO_2. These bands are corresponding to P-O vibration [41]. The broad peak at 1095 cm^{-1} is attributed to the ν3 vibration of the phosphate ions coordinated with TiO_2. The ν2 vibration of the phosphate in a bidentate state (associating at surface) is shown band at 1125 cm^{-1}, and the peak at 1040 cm^{-1} is related to Ti-O-P framework vibrations [42]. It means that P perhaps would exist in the surface as bidentate phosphate and Ti-O-P bonds forming in the lattice [43]. The broad adsorption peak present at 800 cm^{-1} for all materials is assigned to Ti-O-Ti vibration if Ti is in octahedral environment [44].

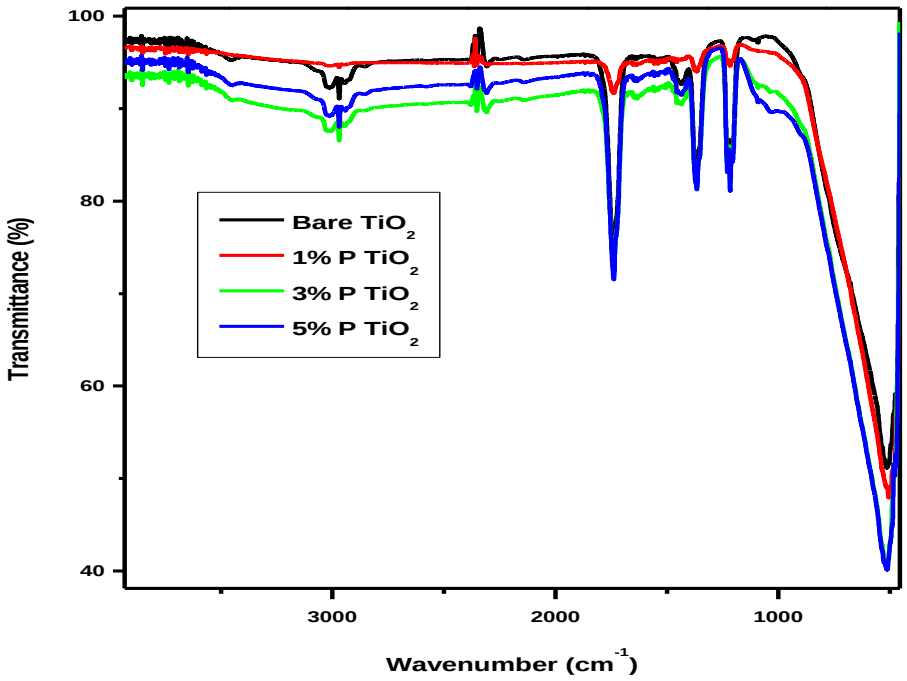

Figure 3: FTIR spectra of bare TiO_2 and P-doped TiO_2 nanoparticles

3.3 Field emission scanning electron microscopy (FESEM)

Morphology of bare TiO_2, 1 mole% and 5 mole % P doped TiO_2 synthesized by using *sol-gel* method and calcined at 500 °C is shown in **Figure 4** (a), (c)and (e) FESEM images shown the surface. It is apparent from these images that the P doped TiO_2 were included of non-spherical particles with an average diameter of 5 - 10 nm of its particle size. The size of particles was estimated by measuring the diameter of the particles from Gaussian fitting of Histograms. **Figure 4** (b, d, f) represents the particle size distribution Gaussian fitting of Histograms, and

average particle size is determined. The histogram shows an average size distribution is 8 nm. The average particle size determined from Gaussian fitting is in close concurrence with the particle size calculated from XRD analysis. The P doped TiO_2 is compared with the bare TiO_2, the diameter and morphology did not change significantly because the amount of P doped on TiO_2 was very less, so the TiO_2 doped of P in the SEM image is difficult to observe effectively. The variation of particle size with mole % of P is shown in **Figure 4**

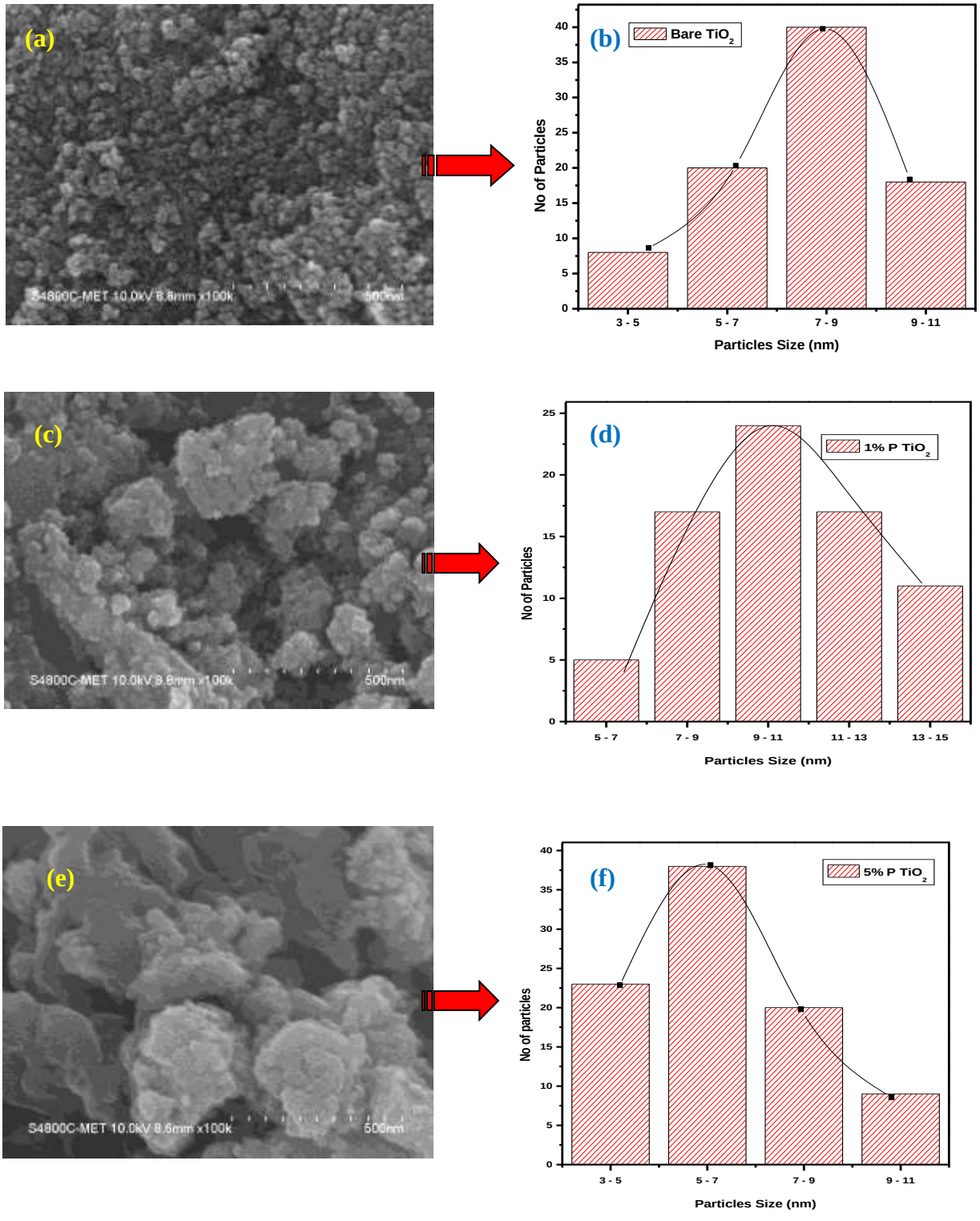

Figure 4: FESEM images of (a) bare TiO_2, (c) 1% P doped TiO_2 and (e) 5% P doped TiO_2 and corresponding histograms of samples (b), (d) and (f)

3.4 EDAX analysis

The elemental composition of P doped TiO_2 spheres with varying amounts of P doping calcined at 500 °C was analyzed using EDAX. EDAX was used to determine the elemental composition of the nanoparticles and the representative patterns are shown in **Figure 5**(a), (b) and (c). These patterns reveal the presence of Ti, P, O elements in the doped samples element. It can be observed that the intensity of the P peak corresponding to emission lines at 2.0 keV(Kα1) increases with increasing P doping by comparing the EDAX spectra of the P doped samples with that of bare TiO_2. The presence of a 0.3, 0.4, 0.5, 0.6, 4.5 and 4.9 keV (Lα1) peaks are attributed to the Ti and O. In **Figure 5** (a), only Ti and O elements were detected in bare TiO_2 powder, while in **Figure 5** (b) and (c), P was detected in addition to Ti and O elements. P doped TiO_2, indicating that P was successfully doped on the TiO_2. Elemental composition of Ti, O and P in weight% and atomic% shown in **Table 2**.

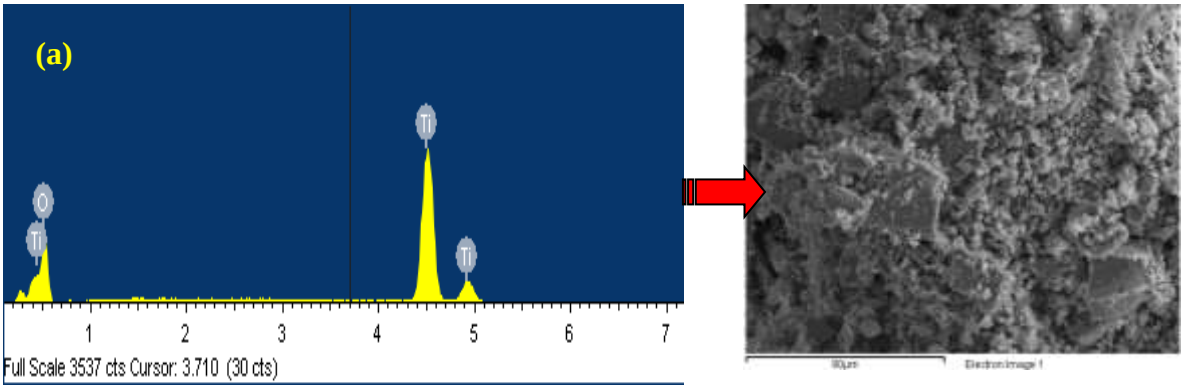

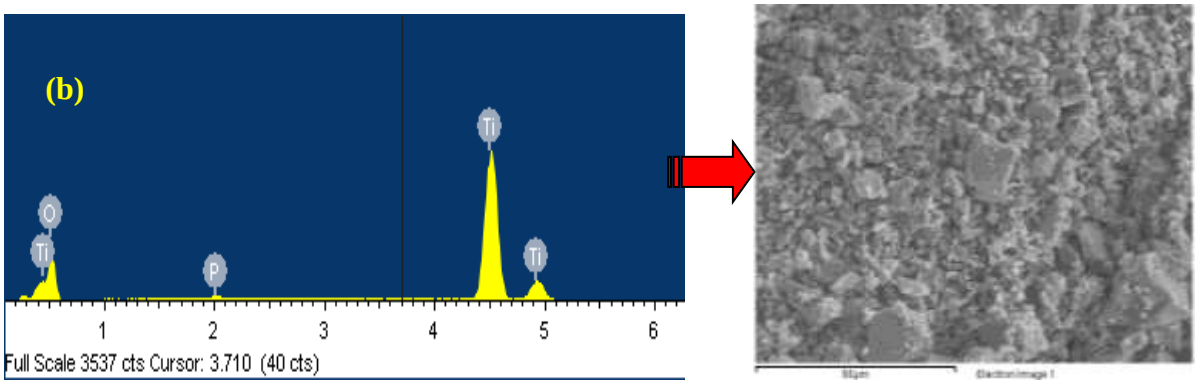

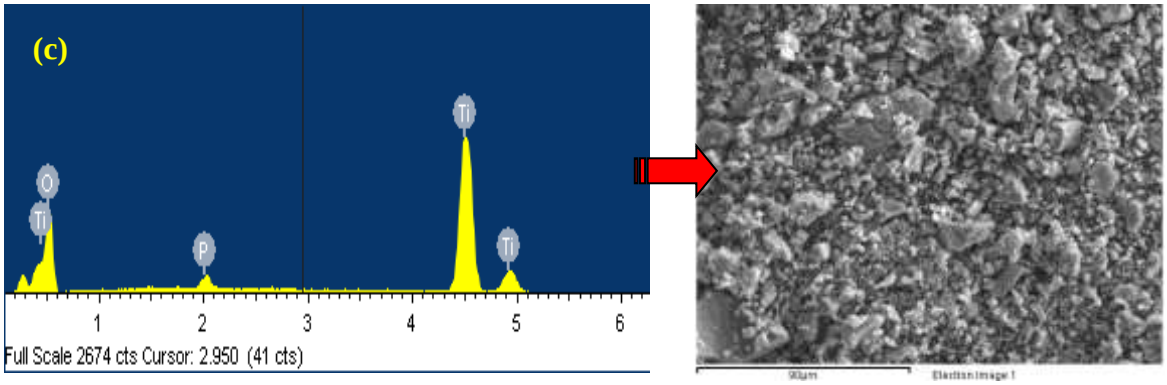

Figure 5: Elemental composition of (a) bare TiO_2, (b) 1% P, and (c) 5% P doped TiO_2 nanoparticles and the representative patterns of EDAX

Table 2: Elemental composition in weight% and atomic%

Sample	Element	Weight%	Atomic%
Bare TiO_2	O K	22.78	46.90
	Ti K	77.22	53.10
	P L	0	0
1 mole % P	O K	18.57	40.52
	Ti K	81.10	59.10
	P L	0.33	0.38
5 mole % P	O K	17.29	38.49
	Ti K	82.06	61.51
	P L	1.42	1.45
Total		100%	

3.5 High resolution transmission electron microscopy (HR-TEM)

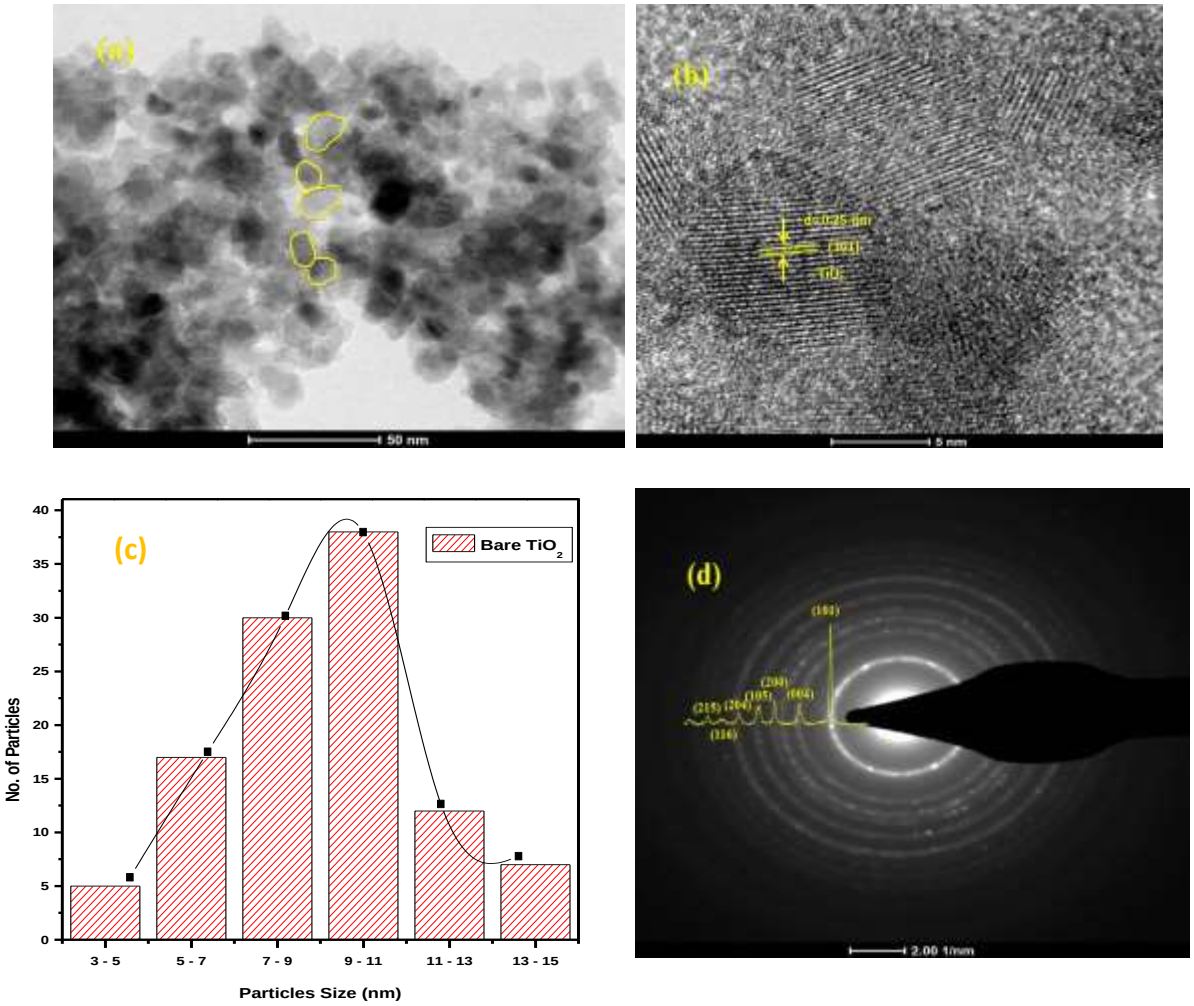

Figure 6 : (a, b, c, d) shows the TEM, High-resolution TEM (HR-TEM), Histogram of particle size and selected area electron diffraction (SAED) pattern for bare TiO_2

HR-TEM technique was used to analyze the surface morphology and particle structure of bare and P doped TiO_2 nanoparticles. The representative HR-TEM images of the bare TiO_2 are shown **Figure 6** (a) to (d) shows the TEM, high-resolution TEM (HR-TEM), histogram of particle size and selected area electron diffraction (SAED) pattern. These images confirm that the bare TiO_2 particles show a spherical-like structure with a size distribution from 9 to 11 nm. While morphological structure of P doped TiO_2 shown in **Figure 7** (a) to (d) confirm that the 5 mole % P doped TiO_2 nanoparticles are elongated-spherical in shape with an average size of 5-7 nm. The nanoparticles are clearly observed in all the images, which shown the high degree of crystallinity. The particle size of 5 mole % P doped TiO_2 nanoparticles are less than that of bare TiO_2 NPs, which is similar with the crystallite size obtained from XRD. Further observation by SAED **Figure 6** (d) and in **Figure 7** (d) confirmed that the nanoparticles are well crystalline in nature with tetragonal anatase structure.

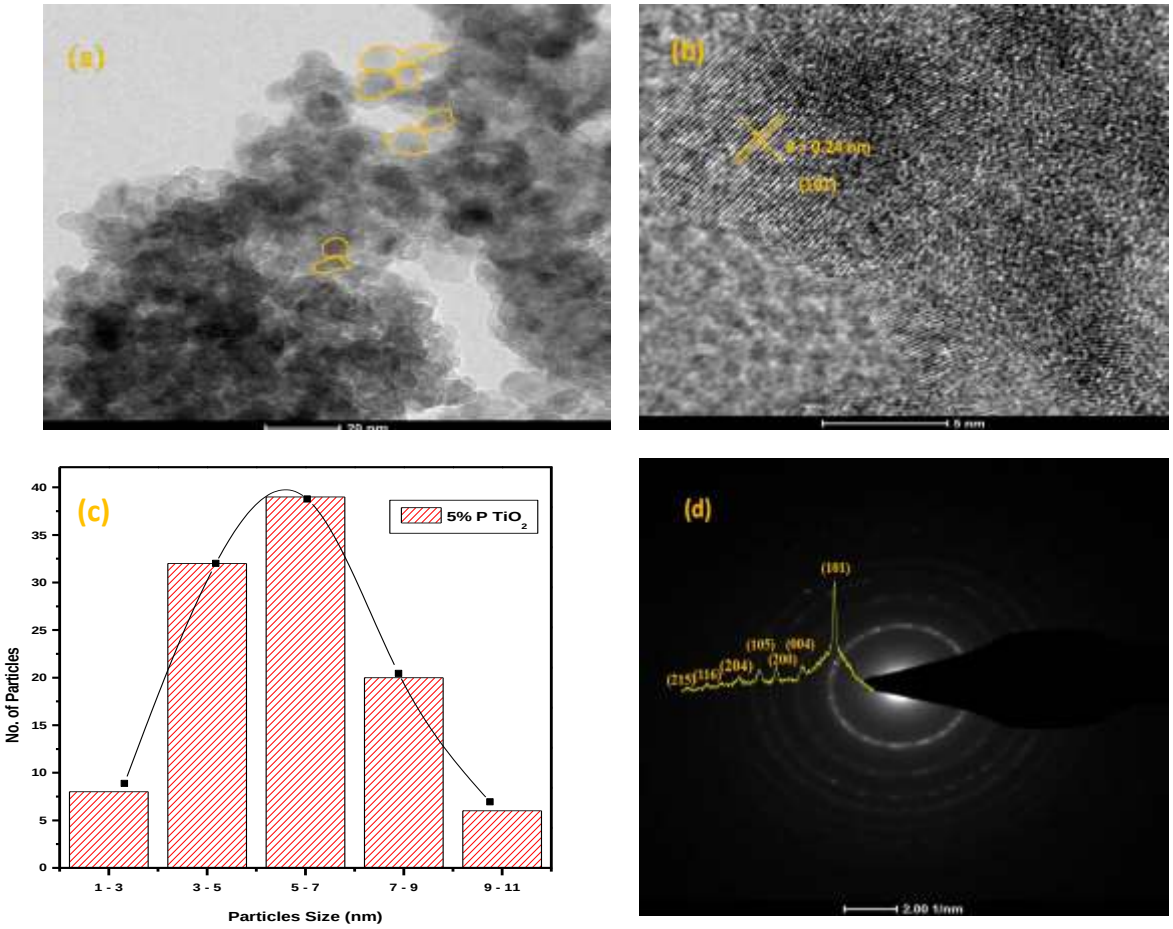

Figure 7 : (a, b, c, d) shows the TEM, High-resolution TEM (HR-TEM), Histogram of particle size and selected area electron diffraction (SAED) pattern for 5 mole% P doped TiO_2

3.6 UV–Visible diffuse reflectance spectroscopy

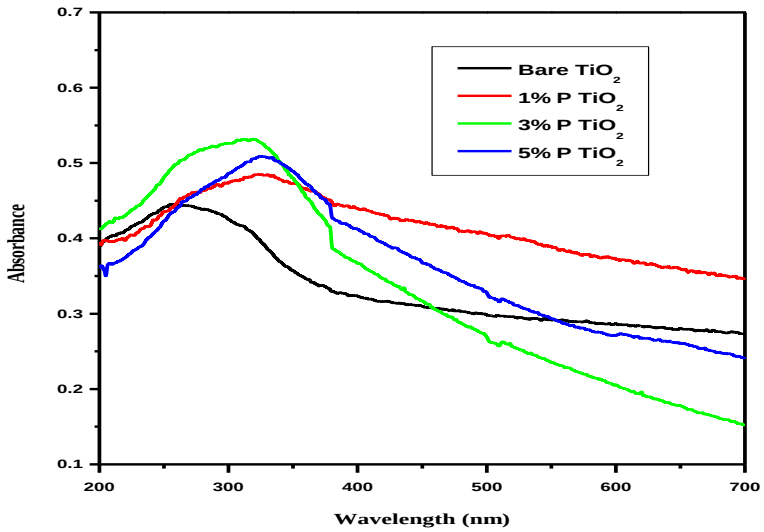

Figure 8: UV-Visible DRS (absorption mode) spectra of bare TiO_2 and 1, 3 and 5 mole % P doped TiO_2 NPs

UV-Visible diffused reflectance spectroscopy (DRS) was used for the investigation of the optical properties and band gap energies of the synthesized materials. **Figure 8** shows the UV-Visible DRS (absorption mode) spectra of bare TiO_2 NPs shows the optical absorption edge in the wavelength region between 250 to 390 nm [45], while compared to P doped TiO_2 (1, 3 and 5 mole % P) shows the shifting its absorption edge from UV to visible region, indicates doping of P in the TiO_2 lattice. As the mole% of P increases in the TiO_2, the visible absorption edge shifted towards higher absorbance as well as higher wavelength region; this is reflected through decrease in the optical band gap. The P-doped TiO_2 samples shown stronger absorption edge in the range of wavelengths from 400 to 550 nm compared to bare TiO_2 [46]. In their electronic structure calculations of phosphorus cation-doped anatase TiO_2 found the band gap narrowing because of the substitution of pentavalent phosphorus (P^{5+}) into Ti^{4+} sites [47].

The optical energy band gap of the P doped TiO_2 was determined by plotting the Tauc plot $(\alpha h\upsilon)^2$ as a function of photon energy ($h\upsilon$) and fixed from the intercept tangent to the x-axis [45] and presented in **Figure 9**.

The energy band gap decreases from 3.2 to 2.0 eV as the doping of mole % of P increases as 1, 3 and 5 mole %. The doping of phosphorous in the TiO_2 lattice, the band gap is lowered to 2.37 eV for 1 mole% P, further reduced to 2.25 eV for 3 mole% P and 2.0 eV for 5 mole% P doping in TiO_2. This absorption enhancement with decrease in band gap in the visible region can be assigned to the formation of dopant level nearer the valance band [48- 50]. The decrease in the optical energy band gap of the P doped TiO_2 NPs, leads to increase in optical absorption.

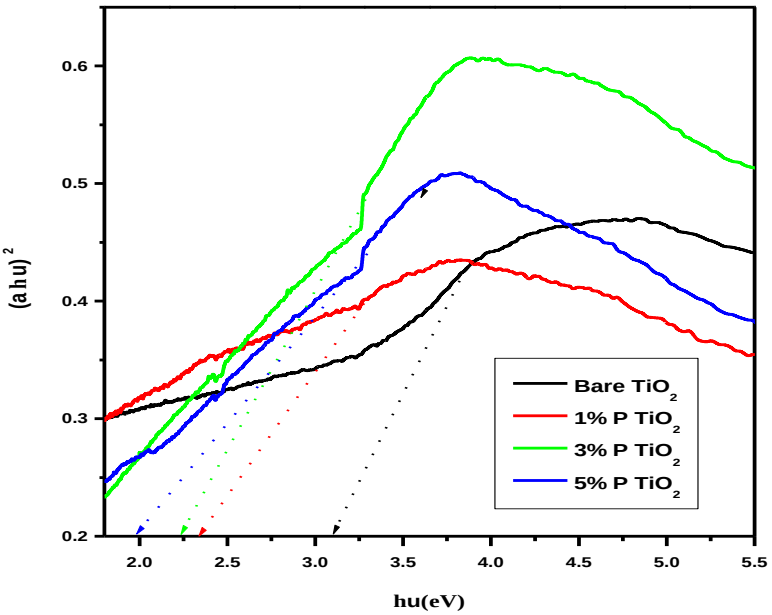

Figure 9: Tauc plot $(\alpha h\upsilon)^2$ as a function of photon energy ($h\upsilon$) of TiO_2 and P doped TiO_2 NPs with 1, 3, and 5 mole % P

4. Conclusion

The experimental results suggest that, the P doped TiO_2 influenced the structural, morphological, and optical properties significantly. UV-DRS studies investigate that the doping of P ion can directly shift band gap of semiconductors into the visible region. The energy band gap decreases from 3.2 to 2.0 eV as the doping of mole % of P increases as 1, 3 and 5 mole %. P doping can effectively decrease the recombination rate of photogenerated charges in TiO_2. FTIR spectra were investigated, as the mole% of P increases; these bands became broader and stronger than that for the bare TiO_2. The P doping is responsible for high adsorption capacity of the TiO_2 due to their large surface area. The absorption bands shown at 1040, 1095, and 1125 cm^{-1} is attributed to the doped materials, signifying the chemical environment of the P in the TiO_2. These bands are corresponding to P-O vibration. The broad peak at 1095 cm^{-1} is attributed to the $\nu 3$ vibration of the phosphate ions coordinated with TiO_2. The $\nu 2$ vibration of the phosphate in a bidentate state (associating at surface) is shown band at 1125 cm^{-1}, and the peak at 1040 cm^{-1} is related to Ti-O-P framework vibrations. It means that P perhaps would exist in the surface as bidentate phosphate and Ti-O-P bonds forming in the lattice. Morphology of bare and various mole % P doped TiO_2 analyzed by using FESEM images. It is apparent from these images that the P doped TiO_2 were included of non-spherical particles with an average diameter of 5 - 10 nm of its particle size. XRD data were investigate, no peak phase assigned to P was observed with doping concentration, the crystal structure of doped TiO_2 samples shows stability of anatase phase when compared with that of bare TiO_2 sample. EDAX studies revealed that the intensity of the P peak corresponding to emission lines at 2.0 keV(Kα1) increases with increasing P doping by comparing the EDAX spectra of the P doped samples with that of bare TiO_2. The presence of a 0.3, 0.4, 0.5, 0.6, 4.5 and 4.9 keV (Lα1) peaks are attributed to the Ti and O. HRTEM images were investigate the morphology of P doped TiO_2 nanoparticles are elongated-spherical in shape with an average size of 5-7 nm. The particle size of 5 mole % P doped TiO_2 nanoparticles are less than that of bare TiO_2 NPs, which is similar with the crystallite size obtained from XRD.

Acknowledgment

Author deeply acknowledges to C-MET, Pune, Principal, Ramkrishna Paramhansa Mahavidyalaya, Osmanabad and Shri Chhatrapati Shivaji Mahavidyalaya, Omerga for providing the research facilities.

References

[1] Sturini M, Speltini A, Maraschi F, et al. Photolytic and photocatalytic degradation of fluoroquinolones in untreated river water under natural sunlight [J]. Applied Catalysis B: Environmental, 2012, 119: 32-39.

[2] Pfaff G, Reynders P. Angle-dependent optical effects deriving from submicron structures of films and pigments [J]. Chemical reviews, 1999, 99 (7): 1963-1982.

[3] Yuan S, Chen W, Hu S. Fabrication of TiO2 nanoparticles/surfactant polymer complex film on glassy carbon electrode and its application to sensing trace dopamine [J]. Materials Science & Engineering C, 2005, 25 (4): 479-485.

[4] Wu H B, Hng H H, Lou X W. Direct synthesis of anatase TiO_2 nanowires with enhanced photocatalytic activity [J]. Advanced Materials, 2012, 24 (19): 2567-2571.

[5] Peng Y, Le Z, Wen M, et al. Mesoporous single-crystal-like TiO2 mesocages threaded with carbon nanotubes for high-performance electrochemical energy storage [J]. Nano Energy, 2017, 35: 44-51.
[6] Zhao G, Pang H, Liu G, et al. Co-porphyrin/Carbon nitride hybrids for improved photocatalytic CO_2 reduction under visible light [J]. Applied Catalysis B: Environmental, 2016, 200: 141-149.
[7] Bian Z, Zhu J, Li H. Solvothermal alcoholysis synthesis of hierarchical TiO_2 with enhanced activity in environmental and energy photocatalysis [J]. Journal of Photochemistry and Photobiology C: Photochemistry Reviews, 2016, 28: 72-86.
[8] Zhao, Zhao, Xiaoyan, et al. Effect of defects on photocatalytic activity of rutile TiO_2 nanorods [J]. Nano Research, 2015, 8 (12): 4061-4071.
[9] Zhu Y, Wang Y, Ling Q, et al. Enhancement of full-spectrum photocatalytic activity over $BiPO_4$ /Bi_2WO_6 composites [J]. Applied Catalysis B: Environmental, 2016, 200: 222-229.
[10] Xiao S, Zhu W, Liu P, et al. CNTs threaded (001) exposed TiO_2 with high activity in photocatalytic NO oxidation [J]. Nanoscale, 2015, 8 (5): 2899-2907.
[11] Zhang H, Wei J, Dong J, et al. Efficient Visible Light Driven Carbon Dioxide Reduction by a Single Atom Implanted Metal – Organic Framework [J]. Angewandte Chemie, 2016, 128 (46): 14522-14526.
[12] Zhu W, Liu P, Xiao S, et al. Microwave-assisted synthesis of Ag-doped MOFs-like organotitanium polymer with high activity in visible-light driven photocatalytic NO oxidization [J]. Applied Catalysis B: Environmental, 2015, 172: 46-51.
[13] Fujishima A, Honda K. Electrochemical photolysis of water at a semiconductor electrode [J]. Nature, 1972, 238 (5358): 37-38.
[14] Chen X, Mao S S. Titanium Dioxide Nanomaterials: Synthesis, Properties, Modifications, and Applications [J]. Cheminform, 2007, 107 (7): 2891-2959.
[15] Wang Z, Lou X W. TiO_2 nanocages: fast synthesis, interior functionalization and improved lithium storage properties [J]. Advanced Materials, 2012, 24 (30): 4124-4129.
[16] Murphy A B, Barnes P R F, Randeniya L K, et al. Efficiency of solar water splitting using semiconductor electrodes [J]. International Journal of Hydrogen Energy, 2006, 31 (14): 1999-2017.
[17] Xu M, Da P, Wu H, et al. Controlled Sn-Doping in TiO_2 Nanowire Photoanodes with Enhanced Photoelectrochemical Conversion [J]. Nano Letters, 2012, 12 (3): 1503-1508.
[18] Wang Y, Zhang Y Y, Tang J, et al. Simultaneous etching and doping of TiO_2 nanowire arrays for enhanced photoelectrochemical performance [J]. Acs Nano, 2013, 7 (10): 9375-9383.
[19] Hu C C, Hsu T C, Kao L H. One-Step Cohydrothermal Synthesis of Nitrogen-Doped Titanium Oxide Nanotubes with Enhanced Visible Light Photocatalytic Activity [J]. International Journal of Photoenergy, 2012, 2012 (51): 1302-1312.
[20] Sun H, Zhou G, Liu S, et al. Visible light responsive titania photocatalysts codoped by nitrogen and metal (Fe, Ni, Ag, or Pt) for remediation of aqueous pollutants [J]. Chemical Engineering Journal, 2013, 231 (9): 18-25.
[21] Shin S H, Chun H H, Jo W K. Enhanced Photocatalytic Efficiency of N-F-Co Embedded Titania under Visible Light Exposure for Removal of Indoor-Level Pollutants [J]. Materials, 2014, 8 (1): 31-41.

[22] Hamadanian M, Jabbari V, Shamshiri M, et al. Preparation of novel hetero-nanostructures and high efficient visible light-active photocatalyst using incorporation of CNT as an electron-transfer channel into the support TiO_2 and PbS [J]. Journal of the Taiwan Institute of Chemical Engineers, 2013, 44 (5): 748-757.
[23] Ding S, Chen J S, Luan D, et al. Graphene-supported anatase TiO_2 nanosheets for fast lithium storage [J]. Chemical Communications, 2011, 47 (20): 5780-5782.
[24] Yan J, Wu G, Dai W, et al. Synthetic Design of Gold Nanoparticles on Anatase TiO_2 {001} for Enhanced Visible Light Harvesting [J]. Acs Sustainable Chem Eng, 2014, 2 (8): 1940-1946.
[25] Alcadipani R. Hydrothermal Synthesis of Nitrogen-Doped Titanium Dioxide and Evaluation of Its Visible Light Photocatalytic Activity [J]. International Journal of Photoenergy, 2012, 2012 (2): 2058-2069.
[26] Jia T, Fu F, Zhao J, et al. Sonochemical Synthesis, Characterization, and Photocatalytic Activity of N-Doped TiO_2 Nanocrystals with Mesoporous Structure [J]. Materials Technology, 2014, 2014 (6): 372-376.
[27] Fang J, Wang F, Qian K, et al. Bifunctional N-Doped Mesoporous TiO_2 Photocatalysts [J]. Journal of Physical Chemistry C, 2014, 112 (46): 18150-18156.
[28] Peres A, Ron A. N-TiO2 Photocatalysts highly active under visible irradiation for NO_X abatement and 2-propanol oxidation [J]. Catalysis Today, 2013, 206 (1): 19-25.
[29] Shin S W, Lee J Y, Ahn K S, et al. Visible Light Absorbing TiO_2 Nanotube Arrays by Sulfur Treatment for Photoelectrochemical Water Splitting [J]. Journal of Physical Chemistry C, 2015, 119 (24): 13375-13383.
[30] Ma X Z, Jin B, Wang H Y, et al. S-TiO_2 composite cathode materials for lithium/sulfur batteries [J]. Journal of Electroanalytical Chemistry, 2015, 736: 127-131.
[31] Han C, Pelaez M, Likodimos V, et al. Innovative visible light-activated sulfur doped TiO_2 films for water treatment [J]. Applied Catalysis B: Environmental, 2011, 107 (1-2): 77-87.
[32] Khan M, Gul S R, Li J, et al. Variations in the structural, electronic and optical properties of N-doped TiO_2 with increasing N doping concentration [J]. Modern Physics Letters B, 2015, 29 (8): 1550022.
[33] Liu Y, Wu Y, Zhou Y, et al. Direct Synthesis of Urchin-Like N-doped TiO_2 Microstructures with Enhanced Photocatalytic Properties [J]. Transactions of the Indian Ceramic Society, 2016, 75 (3): 155-160.
[34] Huang Z, Feng J, Pan W. Electronic Structure and Optical Properties of N-Doped Anatase TiO_2 by First-Principles Calculations [J]. Rare Metal Materials & Engineering, 2011, 40 (22): 475-477.
[35] Kuo C Y, Wu C H, Wu J T, et al. Synthesis and characterization of a phosphorus-doped TiO_2 immobilized bed for the photodegradation of bisphenol A under UV and sunlight irradiation [J]. Reaction Kinetics, Mechanisms and Catalysis, 2015, 114 (2): 753-766.
[36] Elghniji K, Soro J, Rossignol S, et al. A simple route for the preparation of P-modified TiO_2 : Effect of phosphorus on thermal stability and photocatalytic activity [J]. Journal of the Taiwan Institute of Chemical Engineers, 2012, 43 (1): 132-139.
[37] Pan X, Yang M Q, Fu X, et al. Defective TiO_2 with oxygen vacancies: synthesis, properties and photocatalytic applications [J]. Nanoscale, 2013, 5 (9): 3601-3614
[38] Li X, Song J, Liu Y, et al. Controlling oxygen vacancies and properties of ZnO [J]. Current Applied Physics, 2014, 14 (3): 521-527.

[39] L. Wang, Y. Yamauchi, Chemistry of Materials, 21 (2009) 3562.
[40] Lertpaitoonpan W, Ong S, Moorman T (2009) Effect of organic carbon and pH on soil sorption of sulfamethazine. Chemosphere 76:558– 564. https://doi.org/10.1016/j.chemosphere.2009.02.066
[41] Xia Y, Jiang Y, Li F (2014) Effect of calcined atmosphere on the photocatalytic activity of P-doped TiO_2. Appl Surf Sci 289:306–315. https://doi.org/10.1016/j.apsusc.2013.10.157
[42] Elghniji K, Soro J, Rossignol S, Ksibi M (2012) A simple route for the preparation of P-modified TiO_2: effect of phosphorus on thermal stability and photocatalytic activity. J Taiwan Inst Chem Eng 43: 132–139. https://doi.org/10.1016/j.jtice.2011.06.011
[43] Körösi L, Papp S, Bertóti I, Dékány I (2007) Surface and bulk composition, structure, and photocatalytic activity of phosphate-modified TiO_2. Chem Mater 19:4811–4819. https://doi.org/10.1021/cm070692r
[44] Yu J, Zhang L, Zheng Z, Zhao J (2003) Synthesis and characterization of phosphated mesoporous titanium dioxide with high photocatalytic activity. Chem Mater 15:2280–2286. https://doi.org/10.1021/cm0340781
[45] G. Cheng, M. S. Akhtar, O.-B. Yang, F. J. Stadler, *ACS Appl. Mater. Interfaces* 2013, *5*, 6635-6642.
[46] Y. Zhou, Y. Liu, P. Liu, W. Zhang, M. Xing, J. Zhang, A facile approach to further improve the substitution of nitrogen into reduced TiO_2_x with an enhanced photocatalytic activity, Appl. Catal. B Environ. 170e171 (2015) 66e73, http:// dx.doi.org/10.1016/j.apcatb.2015.01.036.
[47] Zheng, R. Y.; Lin, L.; Xie, J. L.; Zhu, Y. X.; Xie, Y. C. J. Phys. Chem. C 2008, 112, 15502
[48] W. Choi, A. Termin, M.R. Hoffmann, J. Phys. Chem. 98 (1994) 13669.
[49] T. Umebayashi, T. Yamaki, H. Itoh, K. Asai, J. Phys. Chem. Solids 63 (2002) 1909.
[50] J. Ben Naceur, R. Mechiakh, F. Bousbih, R. Chtourou, Appl. Surf. Sci. 257 (2011) 10699.